Korean Journal of Chemical Engineering
https://doi.org/10.1007/s11814-024-00234-x

ORIGINAL ARTICLE

Synthesis and Characterization of Quercetin-Functionalized Gold Nanoparticles for Screening Anticancer Potentials: A Flow Cytometry Approach

Jiyoung Lee[1] · Roopkumar Sangubotla[1] · Jongsung Kim[1]

Received: 24 March 2024 / Revised: 21 June 2024 / Accepted: 19 July 2024

Abstract
The gold nanoparticles (AuNPs) were synthesized via the Turkevich-Frens approach, conjugated with polyphenol moieties named quercetin (Qu), and prepared as Au-Qu NPs. In this study, we investigated the anticancer activity of the Au-Qu NPs through an apoptosis assay and a live/dead staining assay. The cell viability and apoptosis studies of the synthesized AuNPs and Au-Qu NPs were investigated on mouse embryonic fibroblast cells (NIH/3T3) and human cervical cancer cell lines (HeLa). Interestingly, minimal cytotoxicity was observed in 3T3 cells. Also, an apoptosis assay was conducted using the flow cytometry approach to investigate the cell death in both 3T3 and HeLa cells after the treatment of AuNPs and Au-Qu NPs using Annexin-FITC and propidium iodide (PI) dyes. The apoptosis studies were performed in both 3T3 and HeLa cells, and the Au-Qu NPs exhibited a reasonably increased apoptosis of 34.5% in HeLa cells as compared to AuNPs in HeLa cells (32.2%). Thus, the Au-Qu NPs are more suitable for investigating anticancer properties than AuNPs. In addition, Au-Qu NPs are displaying less early apoptosis (40.5%) than AuNPs (54.7%) in 3T3 cells, which suggests that Au-Qu NPs are biocompatible in healthy cells. The live/dead assay results obtained in 3T3 and HeLa cells in a time-dependent manner (0, 6, 12, and 24 h) have demonstrated the potential cell viability and cell toxicity in response to AuNPs and Au-Qu NPs.

Keywords Gold nanoparticles · Quercetin-conjugation · Anticancer · Flavonoids · Apoptosis

Introduction

Nanotechnology is the study of nanoparticles (NPs) that are less than 100 nm in size. NPs have many uses, such as in diagnosis, therapy, and drug development to test for anticancer properties [1]. Especially, drug delivery systems based on the NPs are more superior than the existing conventional drug delivery systems in terms of versatile features. Some of these are strong therapeutic efficacy, high solubility of hydrophobic drugs, an enhanced permeability and retention (EPR) effect, and the ability to control the release of specific drugs at specific sites over time [2]. In addition, their biocompatibility, enhanced surface-to-volume ratio, self-assembly modality, and encapsulation efficiency features have made them an alternative drug delivery system in comparison with the established traditional drug delivery systems [3]. In this regard, metal-based NPs are highly interesting among researchers due to their multifarious applications. For instance, metals like gold (Au), iron (Fe), zinc (Zn), silver (Ag), copper (Cu), barium (Ba), magnesium (Mg), bismuth (Bi), cobalt (Co), cerium (Ce), and calcium (Ca)-based NPs have been found to be effective in cancer therapy [4]. However, Au and Ag-based NPs have been demonstrating their anticancer properties in a variety of cancers [5]. Furthermore, metal-based NPs are indispensable for maintaining homeostasis and can regulate the immune system in cancer patients [6]. Nanotechnology also makes it possible to rebuild metal ions into more useful drugs. This can reduce the harmful effects of drugs that don't work on their intended target and keep the drugs' therapeutic effectiveness [7–10]. In this context, flavonoids are more desirable as functionalizing ligands to modify the physicochemical properties of metal-based NPs [11–13]. Further, their extraordinary biomedical potentials, such as cell cycle-modulating, anti-oxidative, angiogenic inhibitory,

✉ Jongsung Kim
jongkim@gachon.ac.kr

[1] Department of Chemical and Biological Engineering, Gachon University, 1342, Seongnam Daero, Seongnam-Si, Gyeonggi-Do 13120, Republic of Korea

Published online: 29 July 2024

anti-apoptotic, anti-inflammatory, and anti-tumor, validate their usage as popular functional ligands with metal-based NPs. For example, quercetin (Qu) has been effective in delivering anticancer properties owing to its blockage of the cell cycle (G2/M and G1/S phases) and involvement in targeting at a molecular level, such as topoisomerase II, p27, cyclin B, p21, etc. More importantly, Qu can mitigate cancer by involving significant reactive centers such as 3-hydroxyl groups in the hydrogen bonding toward the keto group, the o-dihydroxyl B-ring, and the 4-oxo C-ring with the binding of a 2,3-double bond [14–18]. The interactions of Qu with metal-based NPs like gold NPs (AuNPs) are crucial in enhancing the anticancer properties as compared to the AuNPs or Qu alone [19–21].

In this study, we used the Turkevich-Frens method to make AuNPs. Then, the easy stirring reaction was used to connect Qu to the AuNPs, making Au-Qu NPs. The Au-Qu nanoparticles that were made were tested for their ability to fight cancer using 3T3 cells as a healthy control and HeLa cells as a cancer cell model. We thoroughly investigated the anticancer activity of the Au-Qu NPs by employing live/dead staining and apoptosis assays. Based on studies using fluorescence-activated cell sorting (FACS) to look at apoptosis in HeLa cells, the Au-Qu NPs caused a higher rate of apoptosis (34.5%) than the AuNPs treatment, which caused a lower rate of apoptosis (32.2%). Thus, Au-Qu NPs are suitable nanomaterials for studying anticancer properties. The live/dead microscopy images of HeLa cells (0, 6, 12, and 24 h) further supported the apoptosis findings and pointed to the pronounced cytotoxic effects of Au-Qu NPs in HeLa cells.

Experimental

Materials

The compounds gold (III) chloride trihydrate and trisodium citrate dihydrate were acquired from Sigma Aldrich. Phosphate-buffered saline (PBS) with a concentration of 0.1 M and a pH of 7.4, as well as deionized water, were used in all experiments. Direct use of analytical-grade chemicals avoided purification. Mouse embryonic fibroblast cells (NIH/3T3) and human cervical cancer cell lines (HeLa) were obtained from the Korean Cell Line Bank, South Korea. Nest Scientific, USA, supplied the cell culture flasks. The penicillin—streptomycin solutions and trypsin—EDTA were acquired from Gibco Laboratories in Korea. The fetal bovine serum (FBS) was acquired from Young in Frontier, Korea. LIVE/DEAD™ fixable violet dead cell stain kit (cat. no. L34955) was purchased from Thermo Fisher Scientific (USA). The MTT cell proliferation test kit (Abcam, ab211091) was obtained from Abcam. The Annexin V-FITC Apoptosis Kit (cat. no. K101) was purchased from Bio Vision in Milpitas, USA. The TEM sample grid was acquired from Ted Pella, Inc. (USA). The Spectra/Pro® dialysis membrane with a molecular weight cut-off (MWCO) of 0.5–1 kDa was acquired from Biotech CE Tubing, Spectrum Laboratories, located in South Korea. All chemicals and reagents used were of pharmaceutical grade and were not subjected to additional purification.

Instruments and Measurements

The optical characteristics were assessed using a UV–vis spectrophotometer (Varian Cary 100). The Fourier-transform infrared (FT-IR) measurements were conducted using the Vertex 70 instrument manufactured by Bruker in the United States. The analysis of AuNPs was conducted using the Thermo Scientific K-Alpha™ X-ray photoelectron spectrometer. The X-ray diffraction (XRD) pattern for AuNPs was examined using a Rigaku Ultima IV diffractometer. The scan range for the XRD analysis was from $2\theta = 20$ to 90°. TEM images were obtained using a JEM 3010 microscope manufactured by JEOL Ltd.

Synthesis of AuNPs

The AuNPs were synthesized by following the recently reported method via the Turkevich-Frens approach [22, 23]. The solution of $HAuCl_4$ (30 mL, 1.0 mM) was subjected to heating at a temperature of 180 °C while being stirred at a speed of 100 rpm for a duration of 35 min. Following immediate stirring, a 2 mL solution of 1% TCD was added and stirred at a rate of 100 rpm for a duration of 10 min. The appearance of a red-colored solution indicated the creation of AuNPs.

Preparation of Au-Qu NPs

The Au-Qu NPs were synthesized by modifying the earlier report [24]. A solution of Qu (5 mg) was prepared by mixing it with ethanol (30 mL) in a beaker and subjecting it to ultrasonication for 10 min at room temperature. To conjugate, the aforementioned solution (30 mL) was combined with the AuNPs solution (30 mL) and stirred continuously for 2 h using a magnetic stirrer at room temperature. The Au-Qu NPs were subjected to purification by passing them through

a 0.22 µm syringe filter. Subsequently, they were dialyzed for 48 h using DI water and a cellulose ester membrane with a molecular weight cut-off of 0.5–1 kDa. This process was carried out to eliminate any remaining unreacted Qu and AuNPs. The Au-Qu NP solution obtained was stored in the refrigerator for subsequent investigations.

Cell Culture

The HeLa cells were acquired from the Korean Cell Line Bank, South Korea, and were cultivated in Dulbecco's Minimum Essential Medium (DMEM) supplemented with 10% fetal bovine serum (FBS) and 1% penicillin–streptomycin. Subsequently, they were incubated at ideal conditions of 5% CO_2 and 37 °C. After achieving a cell confluency of around 70–90%, the HeLa cells were subcultured. NIH/3T3 cells, which are derived from mouse embryonic fibroblasts, were also bought from the Korean Cell Line Bank in South Korea and grown in the same way as described above using the same growth medium. These cells were used as a healthy cell control for comparison.

Cell Proliferation Assay by MTT

The HeLa and 3T3 cells were placed in a 96-well plate with the appropriate media and then kept in a controlled environment with 5% CO_2 and a temperature of 37 °C for 24 h. The medium was substituted with treatments and fresh medium until the cell confluency reached 50%. In the study, HeLa and 3T3 cells were treated with different amounts of AuNPs and Au-Qu NPS, starting from 0 to 100 µM with 20-µM increments. The cells were cultured under ideal conditions, with 5% CO_2 and a temperature of 37 °C, for a duration of 24 h. Subsequently, the medium was extracted, and 50 µL of both MTT reagent and serum-free media were introduced. The mixture was then incubated for a maximum of 3 h under ideal conditions of 5% CO_2 and 37 °C. Following incubation, the MTT solvent (150 µL) was substituted, and the plate was covered with aluminum foil. The cell viability was determined using a microplate reader with an absorbance of 590 nm [25].

Apoptosis Assay by Flow Cytometry

Cell death analysis was investigated by staining cells with Annexin V-FITC and propidium iodide (PI) as per the protocol. We maintained 4×10^5 cells in 6-well plates and allowed them to grow for 24 h with different amounts of AuNPs and Au-Qu NPs (0, 20, 40, 60, 80, and 100 µM). After 24 h, the 6-well plate was taken out of the incubator and trypsinized in Eppendorf tubes (1.5 mL). The cells were then washed with DPBS and centrifuged at 3000 rpm for 5 min. Once the pellet was obtained, the trypsin was removed and fresh medium (0.5 mL) was added to each tube. The cells were then resuspended in 500 µL of binding buffer and Annexin V-FITC (5 µL) and PI (5 µL) were added, and the tubes were left to sit at room temperature for 5 min in the dark. Then, cells were assessed using a flow cytometer (BDAccury6; Becton Dickinson, USA) and analyzed using FlowJo Software (USA).

Live/dead Cell Staining Assay

Cells were cultured in a 6-well plate for 24 h (5% CO_2; 37 °C) in an incubator. Further, the cells were treated with the AuNPs and Au-Qu NPS (100 µM) for 40 min. Following the incubation, cells were washed and trypsinized by adding trypsin–EDTA (0.5 mL) into each well, kept for CO_2 incubation for 5 min, and added fresh medium (0.5 mL) to the Eppendorf tube. Then we collected the trypsin with cells into the EP tubes and centrifuged (3000 rpm; 5 min), and after obtaining the pellet, we removed the trypsin and added the fresh medium (0.5 mL) to each EP tube. Further, we added binding buffer (0.5 mL) to the EP tubes, resuspended the EP tubes, treated them with a diluted violet dye (1 µL) and PI (1 µL), and incubated them at room temperature for 5 min under the dark conditions. Further, a new 6-well plate was covered with cover slips, and the above cell culture solution (0.5 mL) was added to a fresh medium (0.5 mL) and incubated for 30 min. Finally, live and dead staining assays were observed at different time intervals of 0, 6, 12, and 24 h using an EVOS M5000 phase-contrast microscope.

Statistical Analysis

The results in the present article were reported as the mean of three individual studies with the standard deviation (± SD).

Results and Discussion

Material Characterization

The AuNPs that were prepared exhibited a spherical shape and were evenly distributed when observed under the TEM and HRTEM (Fig. 1a–d). The HRTEM image of the AuNPs

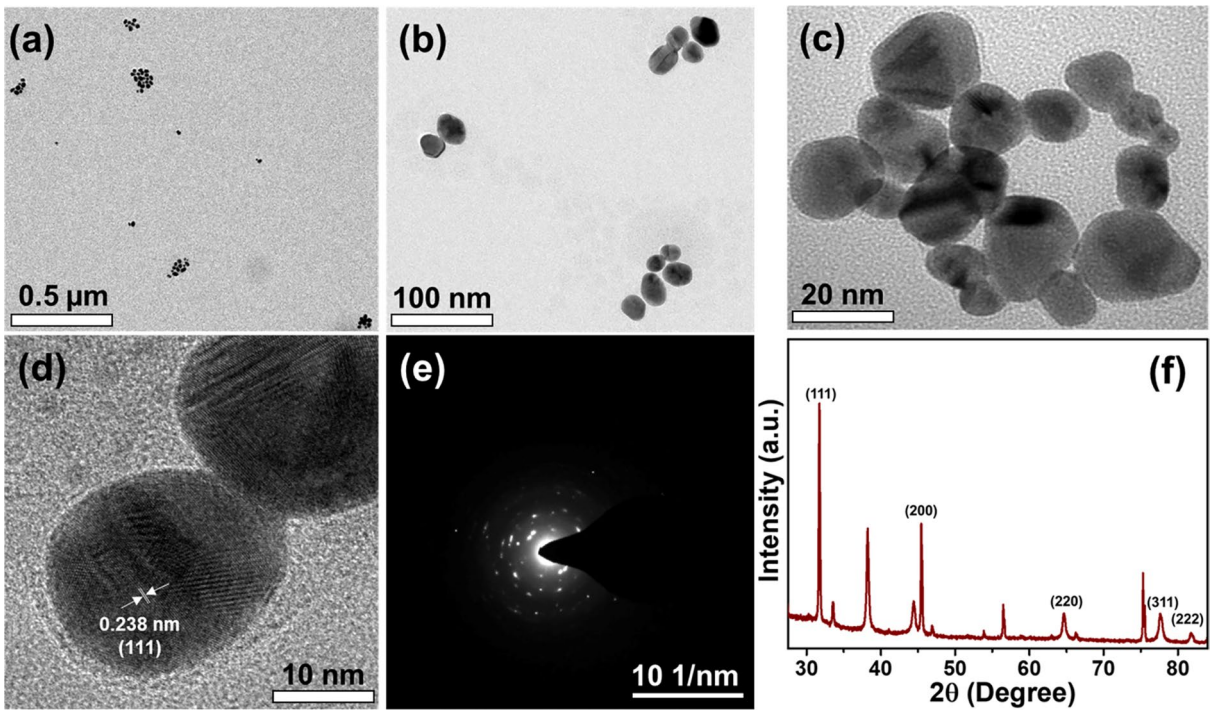

Fig. 1 **a**, **b** TEM images of AuNPs; **c**, **d** HRTEM images of AuNPs, **e** SAED pattern of AuNPs; **f** XRD pattern demonstrating face-centered cubic (fcc) structural features of AuNPs

displayed lattice fringes with an interplanar spacing of approximately 0.238 nm. The fringes were identified as belonging to the lattice plane (111), indicating a face-centered cubic (fcc) crystal phase [26]. Figure 1e displays the selected area electron diffraction (SAED) pattern of AuNPs. This pattern validates the crystallinity seen in the HRTEM investigation. X-ray diffraction analysis was used to study the phase composition of the AuNPs. Figure 1f displays the X-ray diffraction pattern of AuNPs, exhibiting distinct peaks at 31.6°, 45.3°, 64.6°, 77.6°, and 81.6°, corresponding to diffraction planes of (111), (200), (220), (311), and (222). The results were confirmed by high-resolution transmission electron microscopy (HRTEM) images of gold nanoparticles, as well as by previous studies [27, 28].

Figure 2a displays the FT-IR spectra of AuNPs, illustrating stretching vibrations of (O–H) at 3364 cm^{-1}, (C = O) at 1689 cm^{-1}, and (C-O) at 1069 cm^{-1}. The high-resolution XPS spectrum of AuNPs displayed the characteristic Au 4f doublets (Au $4f_{7/2}$ and Au $4f_{5/2}$) with binding energies of 81.1 and 84.7 eV, respectively (Fig. 2b) [29, 30]. AuNPs' optical characteristics were analyzed using UV–Vis absorption spectroscopy, revealing a unique surface plasmon resonance peak at 528 nm (Fig. 2c).

MTT Cell Viability Assay

The MTT assay was used to assess the anticancer properties of AuNPs and Au-Qu NPs in 3T3 and HeLa cells. The cell viability of 3T3 cells was not significantly affected by the produced Au-Qu NPs compared to the AuNPs. The results suggest that the produced Au-Qu NPs could be used in healthy cells without adversely affecting the biologic system. The viability of the HeLa cells has somewhat diminished, suggesting the effectiveness and anticancer capabilities of the Au-Qu NPs (Fig. S1).

Apoptosis Assay by Flow Cytometry

An Annexin-FITC apoptosis test was utilized to study apoptosis in 3T3 and HeLa cells following treatment with AuNPs and Au-Qu NPs. According to the FACS analysis, early apoptotic cell death is not solely determined by the amounts of nanomaterials, but also by the specific type of nanomaterials. Currently, it is not possible to demonstrate concentration-dependent apoptosis. Nevertheless, there appears to be a consistent pattern in the apoptosis process across various cell types and nanomaterials (Au-Qu NPs and Au-Qu NPs) as shown in Fig. S2 and Fig. S3; b-f. The

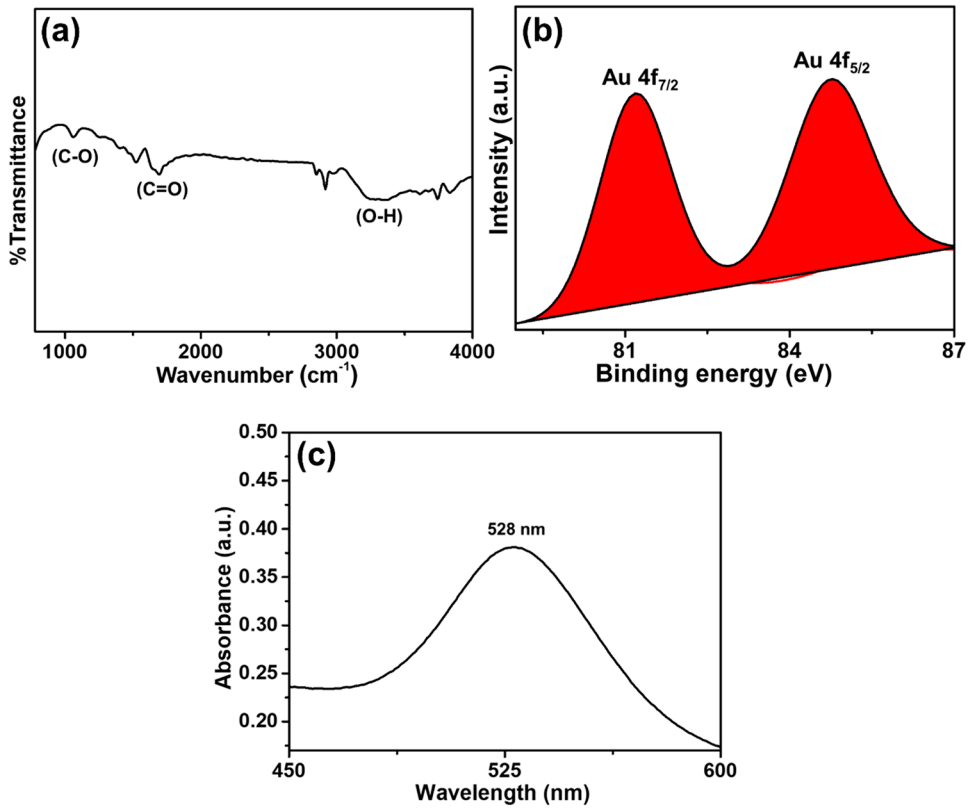

Fig. 2 **a** FT-IR spectrum of AuNPs demonstrating typical stretching vibrations of (O–H), (C = O), and (C–O) functional groups; **b** high-resolution XPS spectrum of Au 4f, and **c** UV–Vis absorption spectrum of AuNPs

Au-Qu NPs, as depicted in Fig. S2g and Fig. S3g, result in a lower rate of early cell death (40.5%) compared to AuNPs (54.7%) in 3T3 cells. Au-Qu NPs are assumed to be equally biocompatible in healthy 3T3 cell lines. The Au-Qu NPs caused a 34.5% increase in apoptosis in HeLa cells, while AuNPs resulted in a 32.2% increase (Figs. 3g and 4g). The produced Au-Qu NPs can be used to explore their anticancer properties. Apoptotic cells can be detected from the binding of annexin V-FITC to phosphotidyl serine (PS) available on the outer side of the cell membrane. In normal cells, PS is predominantly located on cytosolic side of the membrane, and gets translocated near outer portion of the membrane during apoptosis. Early apoptotic cells were stained with annexin V toward negatively charged phospholipid of PS, due to its high affinity. Whereas, in the necrotic cells, the plasma and nuclear membranes are very weakened, and hence, PI may intercalate into the DNA. The obtained FACS Results demonstrate that concentration-dependent increase in apoptotic cells were found and suggesting activation of apoptotic pathways. Also, live–dead analysis was further confirmed these effects, when observed under different time intervals (6, 12, and 24 h) and at high concentrations of Au-Qu NPs (100 µM).

Live/Dead Staining Assay

The reduction in cell viability was found to be influenced by the length of time cells were exposed to AuNPs and Au-Qu NPs. High fluorescence intensity in the blue, green, and red channels suggests increased cell death, while low intensity indicates cell survival. Cell death is influenced by both the time period and the specific cell type, as seen in Fig. S4 and Fig. 5. Greater cell death was noted in HeLa cells compared to 3T3 cells, depending on the duration of time. After 24 h, more cell death was noted in HeLa cells compared to 3T3 cells. Au-Qu NPs have developed into a more efficient anticancer probe when compared to AuNPs.

Conclusion

In this work, we studied the anticancer properties of Au-Qu NPs by conducting apoptosis and live/dead staining experiments. The FACS-based apoptosis tests in HeLa cells showed that Au-Qu NPs caused a significant increase in apoptosis (34.5%) compared to AuNPs (32.2%). Consequently, the functionalized Au-Qu NPs are superior probes

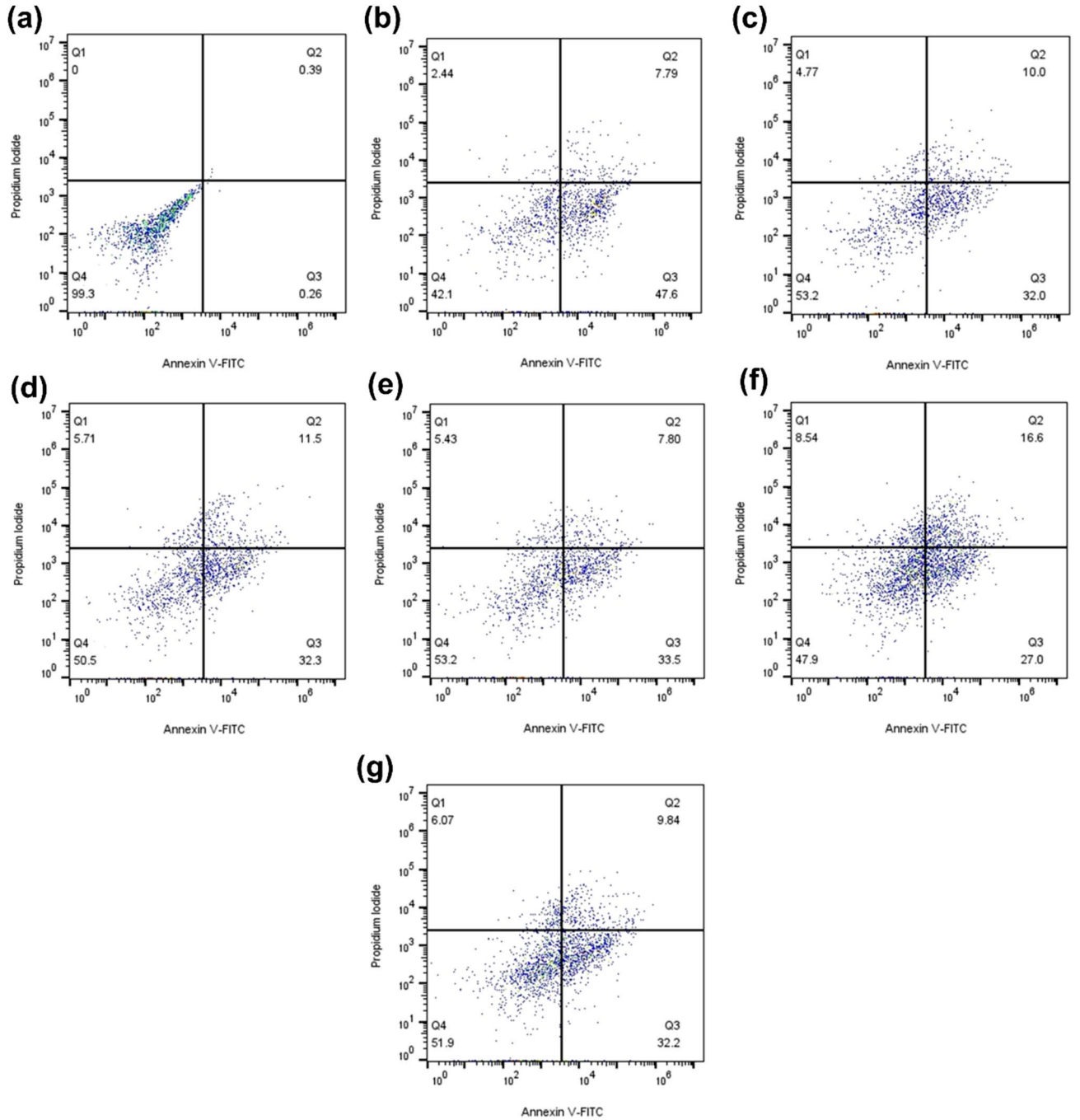

Fig. 3 Flow cytometry analysis of HeLa cells treated with AuNPs. **a** unstained and untreated HeLa cells, and **b** stained and untreated HeLa cells, stained and treated HeLa cells with **c** 20 μM, **d** 40 μM, **e** 60 μM, **f** 80 μM, and **g** 100 μM of AuNPs. Apoptosis dyes include Annexin V-FITC and Propidium Iodine (PI). Q1: FITC-A negative, PI positive (Necrotic cells), Q2: FITC-A positive, PI positive (Late apoptotic cells), Q3: FITC-A positive, PI negative (early apoptotic cells), and Q4: FITC-A negative, PI negative (Viable cells)

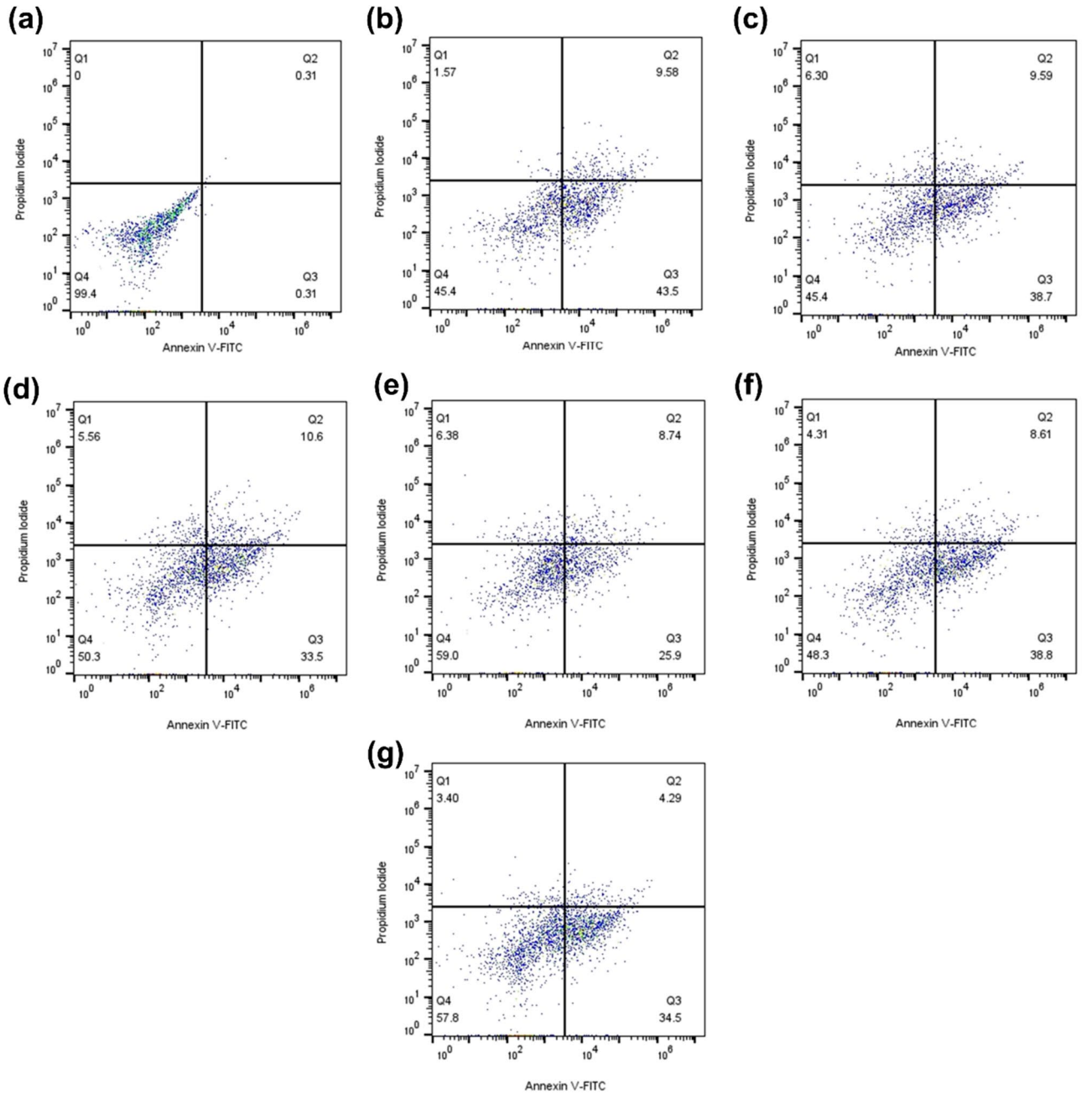

Fig. 4 Flow cytometry analysis of HeLa cells treated with Au-Qu NPs. **a** unstained and untreated HeLa cells, and **b** stained and untreated HeLa cells, stained and treated HeLa cells with **c** 20 µM, **d** 40 µM, **e** 60 µM, **f** 80 µM, and **g** 100 µM of Au-Qu NPs. Apoptosis dyes include Annexin V-FITC and Propidium Iodine (PI). Q1: FITC-A negative, PI positive (Necrotic cells), Q2: FITC-A positive, PI positive (Late apoptotic cells), Q3: FITC-A positive, PI negative (Early apoptotic cells), and Q4: FITC-A negative, PI negative (Viable cells)

for studying anticancer characteristics compared to AuNPs. Furthermore, these findings were supported by live/dead microscopy images of HeLa cells taken at various time points (0, 6, 12, and 24 h). This indicates the possible harmful effects of Au-Qu NPs on HeLa cells.

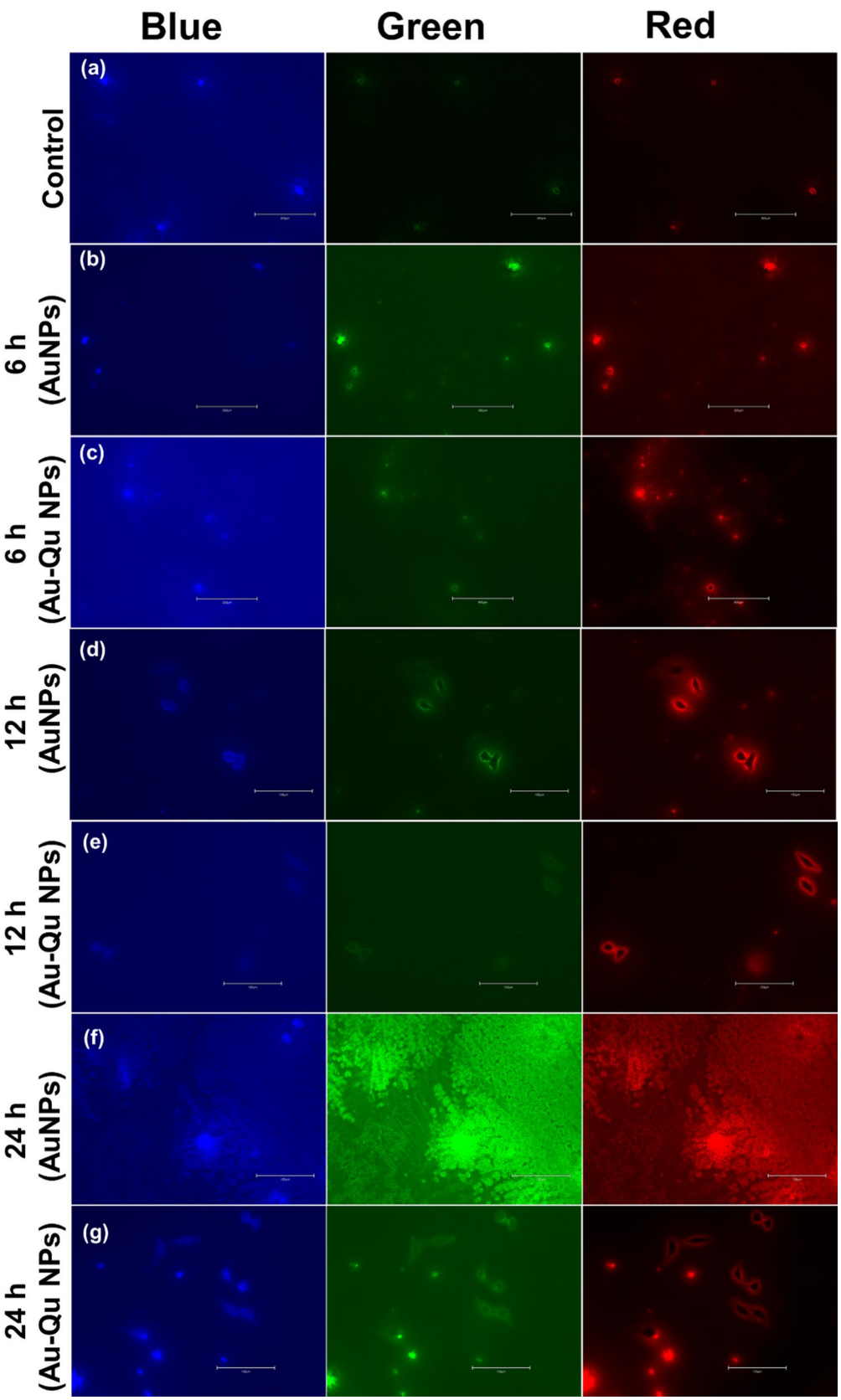
Blue
Green
Red
(a)
Control
(b)
6 h (AuNPs)
(c)
6 h (Au-Qu NPs)
(d)
12 h (AuNPs)
(e)
12 h (Au-Qu NPs)
(f)
24 h (AuNPs)
(g)
24 h (Au-Qu NPs)

◂**Fig. 5** Live/dead cell staining assay images of HeLa cells at regular time intervals about 0, 6, 12, and 24 h. **a** control, **b** at 6 h treated with AuNPs, **c** at 6 h treated with Au-Qu NPs, **d** at 12 h treated with AuNPs, **e** at 12 h treated with Au-Qu NPs, **f** at 24 h treated with AuNPs, **g** at 24 h treated with Au-Qu NPs. The concentrations of AuNPs and Au-Qu NPs were 100 μM each

Supplementary Information The online version contains supplementary material available at https://doi.org/10.1007/s11814-024-00234-x.

Acknowledgements We thank the Smart Materials Research Center for IoT at Gachon University for their technical support with instruments (UV-Vis spectroscopy, FT-IR, and XRD). This work was supported by Basic Science Research Program through the National Research Foundation of Korea (NRF) funded by the Ministry of Education (2021R1A6A1A03038996) and by the National Research Foundation of Korea (NRF) grant funded by the Korea government (MSIT) (NRF-2022R1A2C1009968).

Funding National Research Foundation of Korea (NRF),(2021R1A6A1A03038996),Jongsung Kim,National Research Foundation of Korea (NRF),(NRF-2022R1A2C1009968),Jongsung Kim

Data availability Data related to this article is available on demand.

Declarations

Conflict of interest The authors declare that they have no known competing financial interests or personal relationships that could have appeared to influence the work reported in this paper.

References

1. K. Bromma, W. Beckham, D.B. Chithrani, Cancer Nano. **14**, 80 (2023)
2. H. Sun, Y. Liu, X. Bai, X. Zhou, H. Zhou, S. Liu, B.J. Yan, Mater. Chem. B. **6**, 1633–1639 (2018)
3. E. Jeong, J. Park, H. Kim, S. Lee, Y. Choi, M. Tanaka, J. Choi, Korean J. Chem. Eng. **40**(2), 369–378 (2023)
4. J.J. Xu, W.C. Zhang, Y.W. Guo, X.Y. Chen, Y.N. Zhang, Drug Deliv. **29**, 664–678 (2022)
5. R.H. Taha, Inorg. Chem. Commun. **143**, 109610 (2022)
6. I.H. Suliman, K. Kim, W. Chen, Y. Kim, J.-H. Moon, S. Son, J. Nam, Pharmaceutics. **2023**, 15 (2003)
7. J. Nam, S. Son, K.S. Park, W. Zou, L.D. Shea, J.J. Moon, Nat. Rev. Mater. **4**, 398–414 (2019)
8. T. Fujita, M. Zysman, D. Elgrabli et al., Sci. Rep. **11**, 23129 (2021)
9. K.I. Joo, Korean J. Chem. Eng. **39**, 227–240 (2022)
10. T.V. Dang, M.I. Kim, Korean J. Chem. Eng. **40**, 302–310 (2023)
11. R. Sangubotla, B.A. Lakshmi, S. Kim, J. Kim, Appl. Surf. Sci. **510**, 145417 (2020)
12. A. Zuhrotun, D.J. Oktaviani, A.N. Hasanah, Molecules **28**, 3240 (2023)
13. B.S. Raghavan, S. Kondath, R. Anantanarayanan, R. Rajaram, Process Biochem. **50**, 1966–1976 (2015)
14. B.A. Lakshmi, S. Kim, J.Y. Bae, J.H. An, Inorganica Chim. Acta. **495**, 118989 (2019)
15. A. Parthiban et al., J. Mol. Struct. **1272**, 134167 (2023)
16. P. Rananaware et al., RSC Adv. **12**, 23661–23674 (2022)
17. R.M. Devendiran et al., RSC Adv. **6**, 32560–32571 (2016)
18. M. Yilmaz, ACS Appl. Bio Mater. **2**, 2715–2725 (2019)
19. F.G. Milanezi et al., Saudi Pharm J. **27**, 968–974 (2019)
20. Ozdal Z.D., Sahmetlioglu E., Narin I. et al. 3 Biotech. 9, 212 (2019)
21. K.W. Ren et al., Int. J. Oncol. **50**, 1299–1311 (2017)
22. J. Lee, J. Paul, R. Sangubotla, J. Kim, Phys. Status Solidi A **220**, 2300218 (2023)
23. B. Bartosewicz, K. Bujno, M. Liszewska, B. Budner, P. Bazarnik, T. Płociński, B.J. Jankiewicz, Colloids Surf. A **549**, 25–33 (2018)
24. S. Balakrishnan, F.A. Bhat, P.R. Singh, S. Mukherjee, P. Elumalai, S. Das, C.R. Patra, J. Arunakaran, Cell Prolif. **49**, 678–697 (2016)
25. B.A. Lakshmi, R. Sangubotla, J. Kim, H.T. Ha, S. Kim, Mater. Sci. Eng. C **120**, 111644 (2021)
26. L. Biao, S. Tan, Q. Meng, J. Gao, X. Zhang, Z. Liu, Y. Fu, Nanomaterials **8**, 53 (2018)
27. K. Sneha, N. Sharma, S.V. Sahi, Nanoscale Res. Lett. **9**, 627 (2014)
28. S. Rajeshkumar, J. Genet. Eng. Biotechnol. **14**, 195–202 (2016)
29. A.K. Zak, A.M. Hashim, Ceram. Int. **49**, 18577–18583 (2023)
30. S. Naraginti, Y.J. Li, B, Biol. **170**, 225–234 (2017)